Technical Report

Reaction Mechanisms for Organic Photosynthesis Catalysts

Yoichi MATSUZAKI*

Abstract

In recent years, organic semiconductors have gained much interest as photocatalysts that are key to artificial photosynthesis. However, large portion of the reaction mechanisms of organic photocatalysts remain unclear. In this study, we employed quantum chemical calculations to explore the reaction pathways for the H_2O oxidation and O_2 reduction reactions of resorcinol-formaldehyde resin, a representative organic photocatalyst, and predicted the reaction mechanisms. The reaction intermediates predicted by the calculations could be assigned to multiple signals detected by in situ DRIFTS measurements, demonstrating the validity of the predicted reaction mechanisms.

1. Introduction

Artificial photosynthesis is gaining attention as a technology capable of solving energy and global warming issues. Artificial photosynthesis mimics natural photosynthesis to store solar energy as chemical energy. In natural photosynthesis, water is oxidized to extract electrons, which are then used to reduce CO_2, synthesizing organic matter (storing the aforementioned chemical energy). Artificial photosynthesis extends this process, allowing the reduced substance to be not only CO_2, but also protons (→ producing H_2) or O_2 (→ producing H_2O_2), among others. To make artificial photosynthesis practical, increasing the solar energy conversion efficiency is crucial, and this efficiency heavily depends on the performance of the photocatalyst used. Since the discovery of the Honda-Fujishima effect,[1] inorganic semiconductors have been the mainstream for photocatalysts. Representative examples include the photocatalysts developed by Domen et al.,[2, 3] some of which achieve solar energy conversion efficiencies of 1.1%,[2] approaching the approximately 5% efficiency of biomass.[4] Meanwhile, research on organic catalysts has surged in recent years,[5] with various highly active catalysts reported, including g-C_3N_4,[6, 7] conjugated polymers,[8] covalent organic frameworks (COFs),[9] and resorcinol–formaldehyde (RF) resins.[10] Among them, the RF resin[10] (**Fig. 1**) synthesized by Shiraishi et al. using a high-temperature hydrothermal method generates hydrogen peroxide with an efficiency exceeding 0.5%. Furthermore, the efficiency can be improved to around 1.0% through doping with polythiophene[11] and other methods. Unlike many inorganic catalysts that utilize rare metals, organic catalysts are composed solely of earth-abundant elements (carbon, oxygen, nitrogen, hydrogen, etc.), enabling low-cost mass production. This represents a significant advantage for societal implementation. However, the reaction mechanisms of organic catalysts remain largely unclear, hindering the identification of guidelines for further performance enhancement. Therefore, this study investigates the photocatalytic reaction of RF resin[10] (Fig. 1) with a donor-acceptor structure:

$$2H_2O \rightarrow O_2 + 4H^+ + 4e^- \quad \text{(oxidation reaction)}$$
$$O_2 + 2H^+ + 2e^- \rightarrow H_2O_2 \quad \text{(reduction reaction)}$$

using quantum chemical calculations and experimental methods.

Figure 2 shows an overview of the photocatalytic reaction: ① exciton (electron-hole pairs) generation via photon absorption, ② dissociation of exciton into electron and hole, ③ oxidation of water by hole, and ④ reduction of O_2 by electron. Generally, in organic semiconductors, the large binding energy of exciton makes charge separation difficult. Therefore, approaches such as promoting charge separation through donor-acceptor structures or bulk heterojunctions, and enhancing electron and hole mobility by improving crystallinity, are being investigated.[5] Regarding ③ and ④, while efforts have been made to match the energy levels of the valence and conduction bands with the designated oxidation and reduction poten-

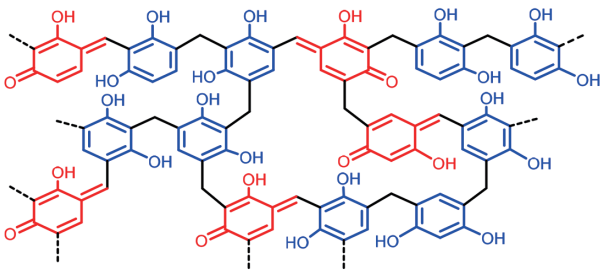

Fig. 1 Molecular structure of resorcinol-formaldehyde (RF) resin

* Dr. Eng., Chief Researcher, Mathematical Science & Technology Research Lab., Advanced Technology Research Laboratories
20-1 Shintomi, Futtsu City, Chiba Pref. 293-8511

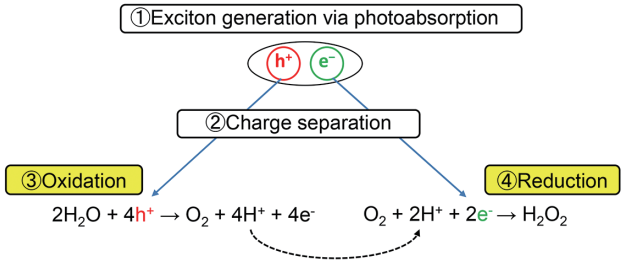

Fig. 2 A schematic representation of the photocatalytic reaction

tials, respectively, more advanced molecular design has been quite restricted due to the unclear reaction mechanisms. Therefore, this study aims to elucidate the mechanisms of the oxidation and reduction reactions occurring after charge separation is achieved.

2. Main Discussion

2.1 Computational methods

Molecular geometry optimizations in the electronic ground state were performed at the CAM-B3LYP/cc-pVDZ level with the SMD solvation model (solvent: H_2O) and D3BJ dispersion correction. Single-point energy calculation was performed using the aug-cc-pVTZ basis set on the basis of the optimized geometries to evaluate activation energies, reaction energies. The Gaussian 16 program[12] was used for these calculations. For benzene dioxide calculations, the Molpro 6.2 program[13] was used to determine the ground state reaction pathway at the CAS(14,12)/6-31G(d) level. Excited state energies along this pathway were calculated at the SA8-CAS(14,12)/6-31G(d) level.

2.2 Mechanism for H_2O oxidation reaction

For metal complexes, which have been extensively studied, both single-site and dual-site mechanisms are known for the H_2O oxidation reaction (**Fig. 3**).[14] Results from this study suggest that the single-site mechanism likely contributes little for RF resin (and probably other organic systems as well). Therefore, the discussion below focuses exclusively on the dual-site mechanism. In part 1 of the oxidation reaction, a proton and an electron are removed from each of two H_2O molecules on the catalyst, leaving two oxygen adatoms on the catalyst (O=M−M=O in Fig. 3). That is, the catalyst's dioxide is formed. However, the O-O bond is not yet formed at this stage; as shown in Fig. 3, O-O bond formation occurs in the subsequent part 2. This stepwise oxygen evolution mechanism is similar to that recently revealed in the Mn cluster of photosystem II in natural photosynthesis,[15] suggesting that O-O bond formation is rather difficult.

Analysis of the H_2O oxidation reaction on the benzenoid and quinonid moieties of RF resin revealed that the former exhibits higher reactivity. Therefore, the reaction mechanism for the benzenoid moiety is described below. Although several types of dioxides exist, the diepoxide (**DE**) primarily contributes to O_2 production. Thus, quantum chemical calculations were employed to explore the reaction pathways leading to $\mathbf{DE}_{min}$, the most stable isomer of **DE**. The results are shown in **Fig. 4**. Here, E_a denotes the activation energy (kcal/mol), and ΔE represents the reaction energy (kcal/mol). We assumed that hole injection occurs first in each step, and the reaction proceeds in the cationic state. The hole was assumed to be injected from any **RF**s into the active unit. The ΔE for the electron emission reaction was calculated as ΔE=IP(reactant)−IP(**RF**), based on the calculated ionization potentials (IP). For the reaction after hole injection, a model was used that included two H_2O molecules forming hydrogen bonds with the H_2O molecule directly involved in the reaction. The activation energy (E_a) for each step was defined as the energy of the transition state relative to the reactant complex. ΔE was defined as ΔE=(total energy of the right side)−(total energy of the left side) for the following reaction equation. X represents the active unit.

Reaction of the red line in Fig. 4:

$$X^+ + H_2O + H_2O(H_2O)_2 \rightarrow X\text{-}OH + H_3O^+(H_2O)_2$$

Figure 4 green line reaction:

$$X\text{-}OH^+ + H_2O(H_2O)_2 \rightarrow X\text{-}O + H_3O^+(H_2O)_2$$

Note that the values in parentheses for ΔE in Fig. 4 denote the total ΔE including that of the preceding hole injection.

Regarding Part 1, step 1 and step 1', calculations for TiO_2 have predicted that, H_2O first adsorbs onto the TiO_2 surface, followed by the removal of a proton and an electron.[16] However, for RF resin, even in the cationic state, H_2O does not adsorb. As seen from the transition state structure (**Fig. 5**, left), the formation of the C-O bond proceeds simultaneously with the transfer of the proton and electron. This indicates it is a type of proton-coupled electron transfer (PCET) reaction, where the motion of the carbon and oxygen nuclei is also coupled. The activation energies (E_a) for both step 1 and step 1' in Fig. 4 are below 20 kcal/mol, suggesting these reactions proceed readily even at room temperature. For comparison, calculations for a reaction analogous to step 1 in the electrically neutral state (in this case, generating an **R1** anion) predicted an E_a of 43 kcal/mol, confirming that this reaction occurs only in the cationic state.

Step 2a (Step 2a') of oxidation reaction part 1 involves the generation of a diol (**DO**) through a reaction similar to Step 1, while Step 2b (Step 2b') involves the generation of an monoepoxide (**ME**, **ME'**) through the departure of a proton from the -OH group introduced in Step 1. The transition state structure for Step 2b is shown on the right in Fig. 5. In both cases, it is a PCET reaction where electrons transfer from the OH group to the RF resin. Focusing on the radical intermediates (**R1**, **R1'**) that initiate the reaction, the IP varies significantly depend on the substitution site of the -OH group. A larger IP makes it harder to accept a hole, but the subsequent

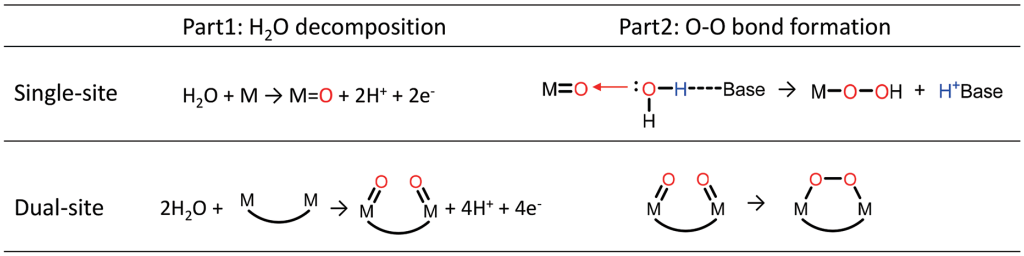

Fig. 3 Mechanism for H_2O oxidation reactions by metal complexes

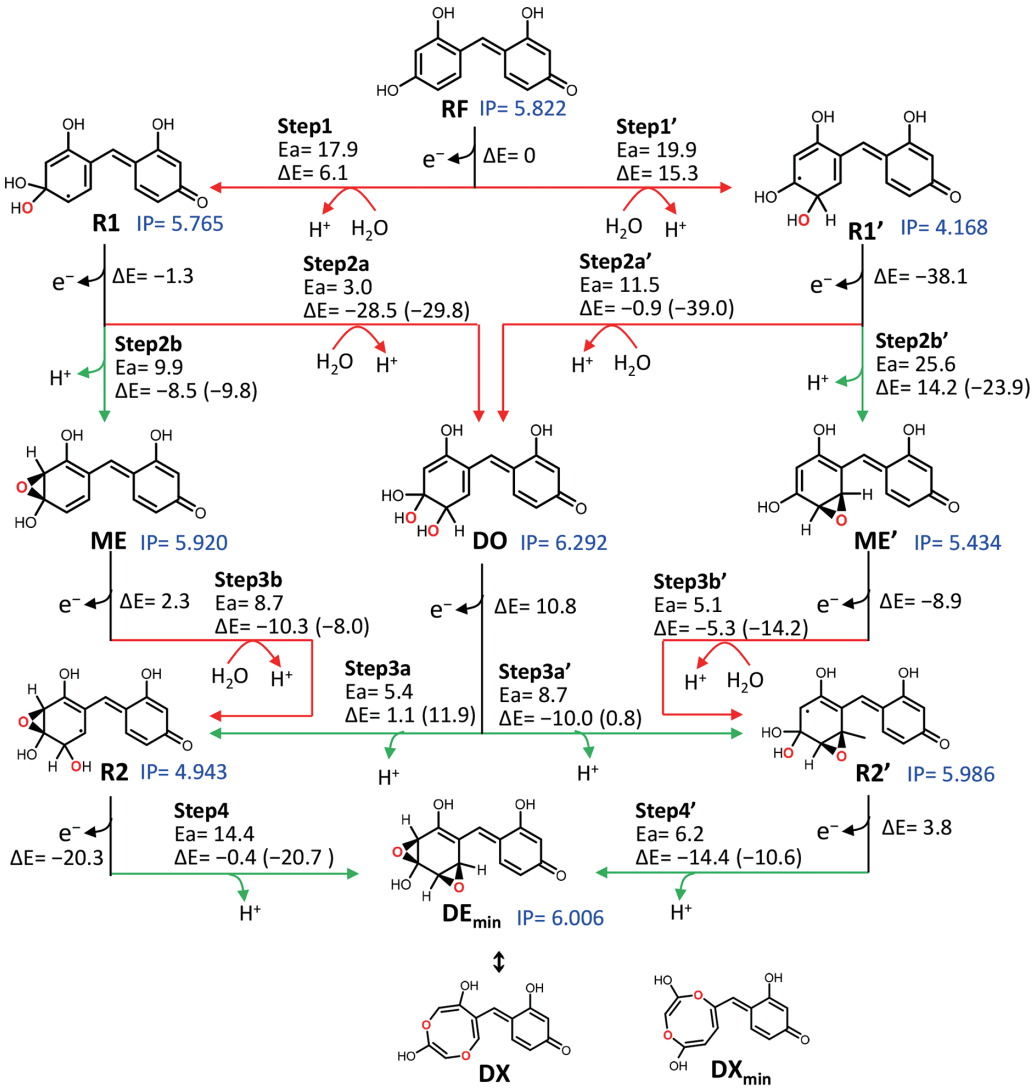

Fig. 4 Mechanism for H_2O decomposition reactions on RF resin

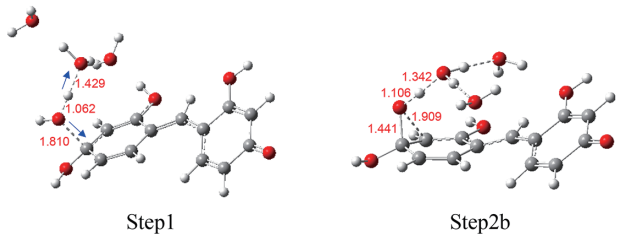

Fig. 5 Calculated transition-state structures for the elementary reaction steps in Fig. 4

PCET reaction is expected to proceed more readily. Indeed, comparing reactions of the same type for **R1** and **R1'** (step 2a and step 2a', step 2b and step 2b'), **R1** with the larger IP exhibits a smaller E_a. This indicates a trade-off relationship between hole injection efficiency and PCET reactivity, representing a key consideration in material design. As shown in Fig. 4, **DO** dominates over **ME** and **ME'** in this system both kinetically and thermodynamically. Although **DO** likely exhibits slower hole injection due to its relatively large IP, the third step (step 3a, step 3a') has a low E_a, suggesting rapid reaction after hole injection. For the fourth step from **R2** or **R2'** to $\mathbf{DE}_{min}$, step 4' with the larger initial IP is faster than step 4, confirming the trade-off relationship observed in the second step. Note that **DE** is tautomeric with dioxocine (**DX**).[17] While **DX** shown in Fig. 4 is 7.4 kcal/mol less stable than $\mathbf{DE}_{min}$, comparing their respective most stable isomers reveals **DX** is 7.0 kcal/mol more stable. Since **DX** cannot be a precursor for O_2 generation, molecular design favoring equilibrium toward the **DE** side might be effective for enhancing catalytic activity.

Some previous studies have suggested that endoperoxide (**1,2-EP**) is generated directly from **R2** or **R2'**.[18] However, according to the present study, **1,2-EP** is 37.4 kcal/mol less stable than $\mathbf{DE}_{min}$. Therefore, the E_a for the reaction from **R2'** to **1,2-EP** is estimated to be at least 43 kcal/mol (calculated by adding the aforementioned 37.4 kcal/mol to the E_a of 6.2 kcal/mol for the reaction from **R2'** to $\mathbf{DE}_{min}$). This suggests the reaction is unlikely to proceed at room temperature. In other words, similar to metal complexes and natural photosynthesis, it was found that a reaction intermediate without O-O bond is initially formed.

Although first-principles calculations in Reference 19) also predicted **DE** formation, the reaction mechanism from **DE** to O_2 release was not described at all. In this study, we first explored the reaction pathway from $\mathbf{DE}_{min}$ to **1,2-EP** via O-O bond formation, followed by O_2 elimination in the electronic ground state. As shown in **Fig. 6**, the formation of **1,2-EP** proceeds in three steps: two epoxide ring-opening reactions (TS1, TS2) and O-O bond formation (TS3). However, the activation energy for the first step is quite large (44.3 kcal/mol), indicating this reaction does not proceed in the ground state.

Therefore, to investigate the possibility of the first step proceeding in the electronic excited states, calculations were performed using the model molecule, benzene dioxide. First, the ground-state reaction pathway, similar to that of RF resin, was obtained at the CAS(14,12)/6-31G(d) level. On the basis of this pathway, the excited-state energies were calculated at the SA8-CAS(14,12)/6-31G(d) level. The results shown in **Fig. 7** revealed that the first step proceeds without an energy barrier in the first excited state (S_1). Furthermore, near **BR1**, S_1 and S_0 are energetically nearly degenerate, and a conical intersection CI1 exists in the vicinity of **BR1**. Additionally, near **BR2**, the four states S_0 to S_3 are nearly degenerate, and another conical intersection CI2 exists.[20]

Based on the above findings, the reaction mechanism involving the excited state is estimated as follows. First, after the structural change from $\mathbf{DE}_{min}$ to **BR1** in the S_1 excited state, a nonadiabatic transition from S_1 to S_0 occurs at CI1 or CI2. After transition to S_0, the path leading to **1,2-EP** via TS3 in the rightward direction (Fig. 7) and the path returning to $\mathbf{DE}_{min}$ in the leftward direction compete. It is considered that the path leading to the more stable $\mathbf{DE}_{min}$ is preferred. Furthermore, as shown in Fig. 6, also the auto-oxidation reaction proceeds from **BR2** and the resulting product is found to be 39.3 kcal/mol more stable than $\mathbf{DE}_{min}$. Thus, although the **1,2-EP** formation is unfavorable compared to the competing reactions, it is expected to proceed to some extent and release O_2.

Furthermore, while the S_1 state of benzene **DE** involves a $\pi\pi^*$ transition, its π^* orbital is significantly hybridized with the antibonding σ^* orbital of the epoxy-ring C-O bond (the bond cleaved in Fig. 7). Consequently, the epoxy ring is readily opened in the S_1 state. However, in extended π-conjugated systems like RF resin, the energy of the π^* orbital decreases, suppressing σ^* orbital mixing. Consequently, a certain energy barrier may exist even in the S_1 state.

As shown in Fig. 6, O_2 elimination from **1,2-EP** is a two-step reaction (TS4, TS5), and both steps proceed in the S_0 state at room

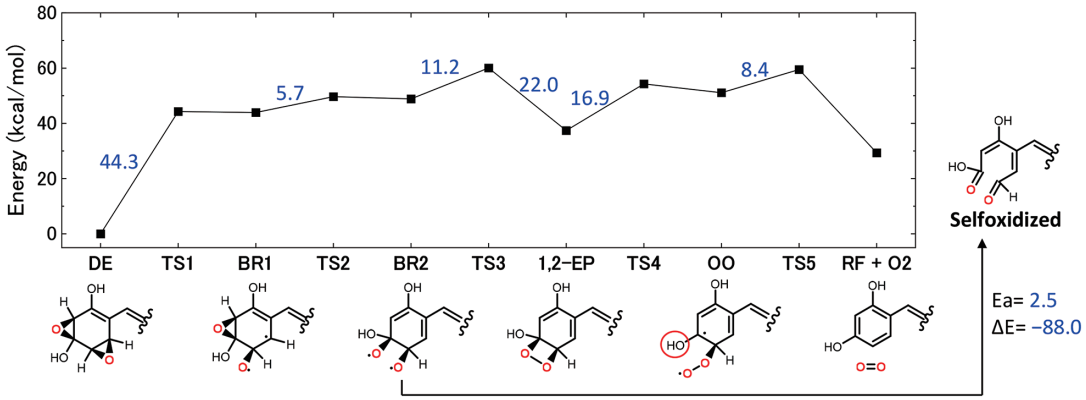

Fig. 6 Calculated potential energy curves along the reaction pathway of O-O bond formation on RF resin

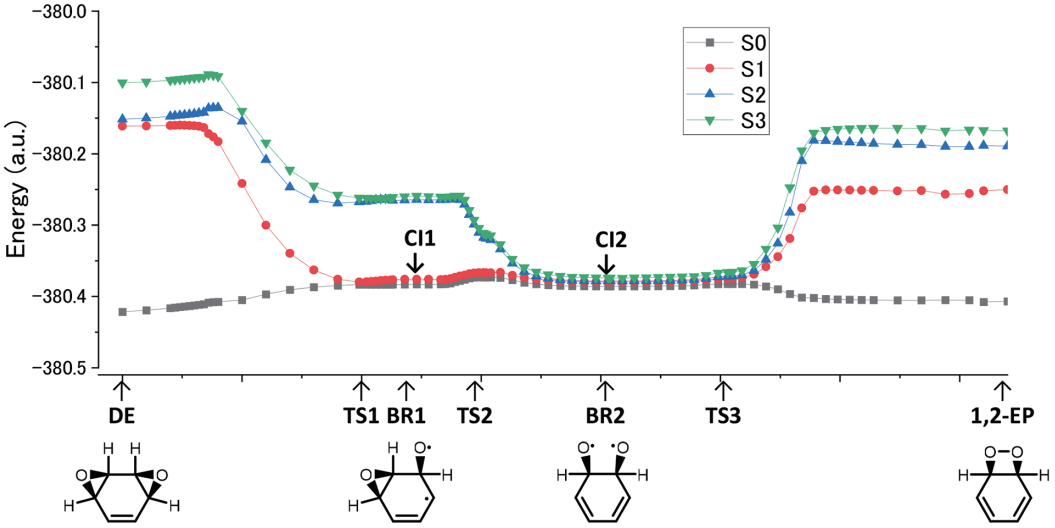

Fig. 7 Calculated potential energy curves for the electronic ground and excited states of benzene dioxide

temperature. In this case, singlet oxygen $^1O_2$ is generated, which is thought to relax to triplet oxygen $^3O_2$ by emitting phosphorescence. Focusing on the reaction starting from **1,2-EP**, the activation energy for conversion to **OO** (16.9 kcal/mol) is smaller than that for conversion to **BR2** (22.0 kcal/mol). Therefore, once formed, **1,2-EP** is likely to preferentially release O_2 rather than proceed toward **DE** or autooxidation products. This situation may also lead to improved catalyst durability.

Regarding the E_a for the O_2 elimination reaction, it was also found that the -OH group in the benzenoid moiety has a significant influence. Computational results revealed that the C-O bond is more easily cleaved at sites substituted with -OH, thereby promoting the O_2 elimination. Specifically, replacing the -OH group (shown as a red circle in Fig. 6) with -H increased the E_a for TS4 to 32.7 kcal/mol. The C-O bond distance in **1,2-EP** is 1.466 Å on the -OH-substituted side and 1.451 Å on the unsubstituted side, suggesting that the bond is weakened on the -OH-substituted side.

2.3 Mechanism for O_2 reduction reaction

There are two major mechanisms for O_2 reduction reaction: the two-step mechanism

$$O_2 + e^- \rightarrow O_2^- \quad (1)$$

$$O_2^- + 2H^+ + e^- \rightarrow H_2O_2 \quad (2)$$

and the one-step mechanism

$$O_2 + 2H^+ + 2_e^- \rightarrow H_2O_2 \quad (3)$$

For RF resin, since the conduction band energy level (0.21 V vs RHE (Reversible Hydrogen Electrode)) is less negative than the potential (−0.33 V) of (1), no contribution from a two-step mechanism is expected. Indeed, the ·OOH radical predicted in the process (2) was not detected by ESR (Electron Spin Resonance) measurements. Therefore, the O_2 reduction by RF resin is expected to follow a one-step mechanism. In the one-step mechanism, the O_2 molecule first adsorbs onto the catalyst and then accepts electrons and protons on the catalyst.

First, we examined the O_2 adsorption on all atomic sites of electrically neutral RF resin. The results showed that either no O_2 adsorption structure could be determined, or while an adsorption structure was determined, the binding energy was negative. Therefore, we concluded that O_2 does not adsorb on electrically neutral RF resin. On the other hand, in the field of O_2 reduction electrode catalysts, a mechanism has been proposed where O_2 adsorption is promoted by the formation of a radical.[21] Molecules possessing basic sites, such as nitrogen atoms in heterocycles, can relatively easily accept electrons when a proton is attached to the site and bearing a positive charge. The resulting radical then strongly traps O_2. Since the carbonyl oxygen of RF resin also has a relatively high basicity, we applied the above mechanism to RF resin.

First, calculations of proton binding energies at each atomic site revealed that the carbonyl oxygen exhibits the highest basicity, and the proton addition reaction (the first step in **Fig. 8**) is exothermic. The electron affinity (EA) of the protonated adduct **RFH**$^+$ is approximately 1 eV higher than that of **RF**, leading to preferential electron capture and the generation of the radical species **RFH**. Among the atomic sites of **RFH**, the methine carbon with the highest spin density (Fig. 8) is expected to have the highest affinity for O_2. Calculations showed that the binding energy of O_2 to this site was 18.9 kcal/mol, while the binding energies for other sites were negative. As shown in Fig. 8, the reaction where a hydrogen atom migrates from **RFH** to O_2 forming ·OOH is thermodynamically less favorable than the O_2 binding reaction. This is consistent with the experimental fact that ·OOH was not detected. Since **RFH_OO**, with O_2 bound, has an EA comparable to that of **RFH**$^+$, further reduction of **RFH_OO** is thought to proceed via the sequence: electron injection → proton addition. This results in the formation of a hydroperoxide (**HP**) with -OOH bonded to the methine carbon. Two reaction pathways exist for H_2O_2 release from **HP**, and the proton addition mechanism was found to have lower activation energy than the intramolecular reaction mechanism. Based on the above, RF resin is thought to reduce O_2 to H_2O_2 via the catalytic reaction cycle shown in red in Fig. 8.

2.4 Verification by DRIFTS measurement

Based on the above considerations, the proposed photocatalytic reaction mechanism for RF resin is shown in **Fig. 9**. To verify this, in-situ DRIFTS (Diffuse reflectance infrared Fourier transform spectroscopy) measurements were performed under photoirradiation. **Fig. 10** shows the four new infrared absorptions observed between 1 300 and 1 800 cm^{-1}. By comparing with the IR spectra of reaction intermediates obtained by quantum chemical calculations, the four peaks above were found to be attributable to the reaction intermediates (Fig. 9) as follows.

The shoulder near 1 350 cm^{-1} corresponds to the OOH bending vibration of H_2O_2.[22] Peak ① is located approximately 47 cm^{-1} higher in wavenumber and, according to our calculations, is assigned to the OOH bending vibration of **HP**. The wavenumber difference of 35 cm^{-1} from quantum chemical calculations agrees well with the experimental value. Peaks ② and ③ are attributed to the C=C

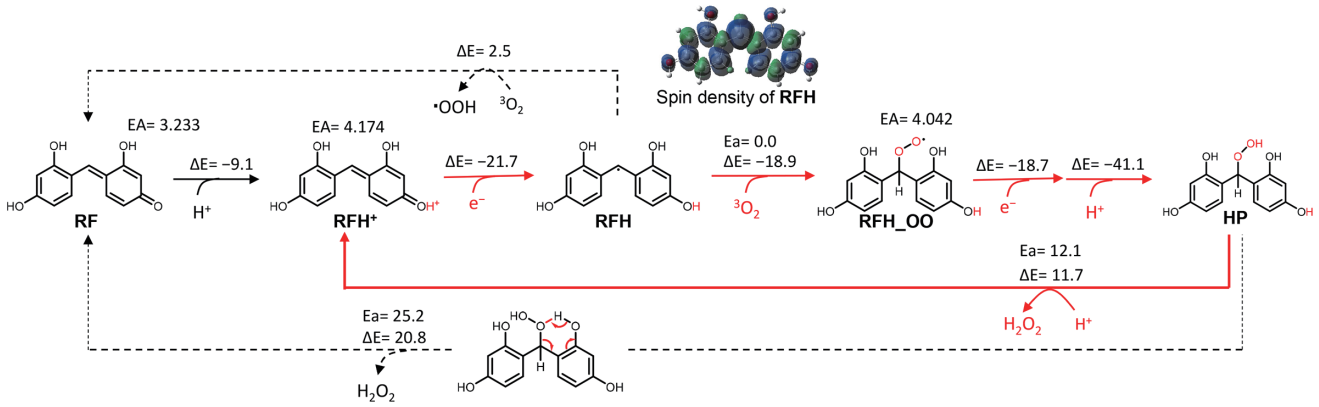

Fig. 8 A possible reaction mechanism for O_2 reduction by RF resin

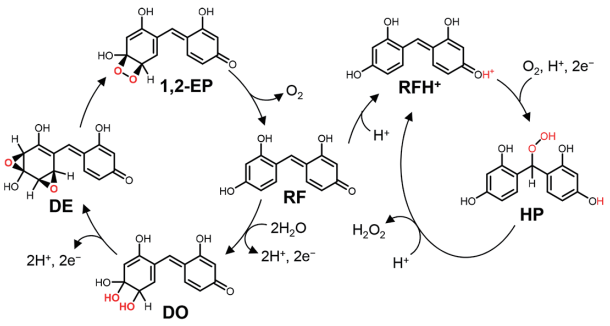

Fig. 9 A possible reaction mechanism for (left) H_2O oxidation and (right) O_2 reduction

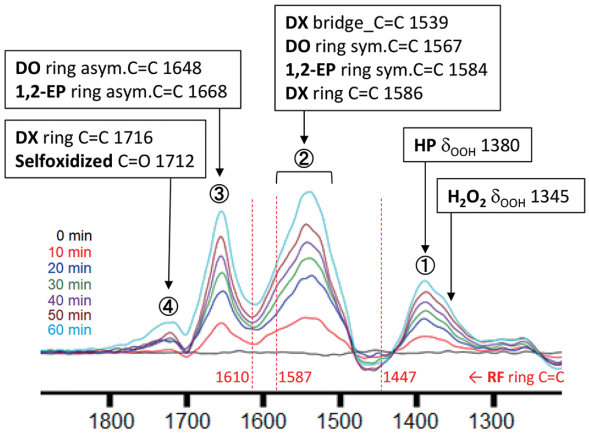

Fig. 10 In situ DRIFTS spectra of a RF resin obtained during photoirradiation (λ>300 nm) of water (200 Pa) and O_2 (200 Pa) at 298 K

stretching vibration in the benzenoid moiety of the reaction intermediate. Although the corresponding vibration in **RF** appears at the wavenumber indicated by the red line in Fig. 10, peaks ② and ③ appear in a different wavenumber region and exhibit significantly increased infrared absorption intensity compared to **RF**. Peak ④ is attributed to the C=C stretching vibration (O-C=C-O) of **DX** and the C=O stretching vibration of the autooxidation product. As described above, the time evolution in the DRIFTS spectrum upon photoirradiation can be attributed to the reaction intermediates, supporting the validity of the proposed reaction mechanism. Furthermore, since the C=C stretching vibration of **DE** is nearly identical to that of **RF** in both frequency (1 609 cm^{-1}) and intensity, it is considered not to contribute to the difference spectrum in the wavenumber region shown in Fig. 10. For **DE**, the vibration of the epoxy ring is expected to appear at 800–1 000 cm^{-1}.

3. Conclusions

Using quantum chemical calculations and DRIFTS measurements, we revealed the mechanisms for the H_2O oxidation and O_2 reduction reactions by resorcinol-formaldehyde resin, a representative organic artificial photosynthesis catalyst. In particular, the photooxidation mechanism of H_2O on organic semiconductors has been rarely reported, and the results of this study are expected to provide important insights for improving photocatalysts.

Acknowledgments

We would like to express our sincere gratitude to Associate Professor Yasuhiro Shiraishi of Osaka University for performing the DRIFTS measurements of RF resin under photoirradiation, and to Professor Yasutaka Kitagawa of Osaka University for his valuable advice regarding the quantum chemical calculations.

References

1) Fujishima, A., Honda, K.: Nature. 238, 37 (1972)
2) Wang, Q., Hisatomi, T., Jia, Q., Tokudome, H., Zhong, M., Wang, C., Pan, Z., Takata, T., Nakabayashi, M., Shibata, N., Li, Y., Sharp, I.D., Kudo, A., Yamada, T., Domen, K.: Nat. Mater. 15, 611–615 (2016)
3) Takata, T., Jiang, J., Sakata, Y., Nakabayashi, M., Shibata, N., Nandal, V., Seki, K., Hisatomi, T., Domen, K.: Nature. 581, 411–414 (2020)
4) Slattery, R.A., Ort, D.R.: Plant Physiol. 168, 383–392 (2015)
5) Banerjee, T., Podjaski, F., Kröger, J., Biswal, B.P., Lotsch, B.V.: Nature Reviews Materials. 6, 168–190 (2021)
6) Wang, X., Maeda, K., Thomas, A., Takanabe, K., Xin, G., Carlsson, J.M., Domen, K., Antonoetti, M.: Nat. Mater. 8, 76–80 (2009)
7) Shiraishi, Y., Kanazawa, S., Sugano, Y., Tsukamoto, D., Sakamoto, H., Ichikawa, S., Hirai, T.: ACS Catal. 4, 774–780 (2014)
8) Sprick, R.S., Bonillo, B., Clowes, R., Guiglion, P., Brownbill, N.J., Slater, B.J., Blanc, F., Zwijnenburg, M.A., Adams, D.J., Cooper, A.I.: Angew. Chem., Int. Ed. 128, 1824 (2016)
9) Wang, C., Lyu, P., Chen, Z., Xu, Y.: J. Am. Chem. Soc. 145, 12745–12754 (2023)
10) Shiraishi, Y., Takii, T., Hagi, T., Mori, S., Kofuji, Y., Kitagawa, Y., Tanaka, S., Ichikawa, S., Hirai, T.: Nat. Mater. 18, 985–993 (2019)
11) Shiraishi, Y., Matsumoto, M., Ichikawa, S., Tanaka, S., Hirai, T.: J. Am. Chem. Soc. 143, 12590–12599 (2021)
12) Frisch, M.J. et al.: Gaussian 16, Revision A.02. Gaussian, Inc., Wallingford, CT, 2016
13) MOLPRO 6.2, a package of ab initio programs, Werner, H.-J., Knowles, P. J. et al: see https://www.molpro.net
14) Shaffer, D.W., Xie, Y., Concepcion, J.J.: Chem. Soc. Rev. 46, 6170–6193 (2017)
15) Suga, M. et al.: Science. 366, 334–338 (2019)
16) Li, Y-F., Selloni, A.: ACS Catal. 6, 4769–4774 (2016)
17) Altenbach, H-J., Vogel, E.: Angew. Chem. Int. Ed. 11, 937–939 (1972)
18) Wang, L., Wan, Y., Ding, Y., Wu, S., Zhang, Y., Zhang, X., Zhang, G., Xiong, Y., Wu, X., Yang, J., Xu, H.: Adv. Mater. 29, 1702428 (2017)
19) Jing, Y., Zhou, Z., Geng, W., Zhu, X., Heine, T.: Adv. Mater. 33, 2008645 (2021)
20) Martínez-Fernández, L., González-Vázquez, J., González, L., Corral, I.: J. Chem. Theory Comput. 11, 406–414 (2015)
21) Takeyasu, K., Furukawa, M., Shimoyama, Y., Singh, S.K., Nakamura, J.: Angew. Chem. Int. Ed. 60, 5121–5124 (2021)
22) Giguère, P-A.: J. Chem. Phys. 18, 88–92 (1950)

Yoichi MATSUZAKI
Dr. Eng., Chief Researcher
Mathematical Science & Technology Research Lab.
Advanced Technology Research Laboratories
20-1 Shintomi, Futtsu City, Chiba Pref. 293-8511